

## Attenuation management in terahertz frequency conversion with temporal boundary using a metallic structure

Fumiaki Miyamaru<sup>1,\*</sup>, Miki Amaki,<sup>1</sup> Keisuke Takano<sup>1</sup>, Joel Pérez-Urquiza<sup>2,3</sup>, Julien Madéo<sup>1,3</sup>, Keshav M. Dani<sup>3</sup>, Yosuke Nakata<sup>4,5</sup>, and Toshihiro Nakanishi<sup>6</sup>

<sup>1</sup>Department of Physics, Faculty of Science, Shinshu University, Nagano 390-8621, Japan

<sup>2</sup>Laboratoire de Physique de l'École Normale Supérieure (ENS), Université PSL, CNRS, Sorbonne Université, Université de Paris, F-75005 Paris, France

<sup>3</sup>Femtosecond Spectroscopy Unit, Okinawa Institute of Science and Technology Graduate University, Okinawa 904-0495, Japan

<sup>4</sup>Graduate School of Engineering Science, Osaka University, Osaka 560-8531, Japan

<sup>5</sup>Center for Quantum Information and Quantum Biology, Osaka University, Osaka 560-0043, Japan

<sup>6</sup>Department of Electronic Science and Engineering, Kyoto University, Kyoto 615-8530, Japan

(Received 31 January 2024; revised 28 March 2024; accepted 29 March 2024; published 24 April 2024)

In this study, we demonstrate the management of terahertz pulse attenuation using a metallic structure in the frequency-conversion process with a temporal boundary. During the propagation of a terahertz pulse, rapid optical excitation of the waveguide surface induces a temporal boundary that can cause frequency conversion. The output amplitude of the terahertz pulse varies depending on the timing of the temporal boundary, which is a notable issue in this process. This is attributed to the difference in the attenuation constants before and after the temporal boundary. We fabricated a waveguide with a metal structure consisting of periodically aligned metal lines. This metallic structure decreases the area in which photo-excited carriers are generated and reduces the attenuation constant after the temporal boundary. On the other hand, the attenuation constant before the temporal boundary increased because of the Joule loss of the patterned metal. These effects balance the attenuation constants before and after the temporal boundary. Consequently, regardless of the location of the terahertz pulse within the waveguide at the timing of the temporal boundary, the amplitude of the output terahertz pulse remained constant.

DOI: [10.1103/PhysRevApplied.21.044044](https://doi.org/10.1103/PhysRevApplied.21.044044)

### I. INTRODUCTION

Over the last two decades, the application of terahertz waves has attracted attention in various scientific and technological fields. In particular, their potential is expected in areas such as wireless communications [1], security inspections [2,3], and chemical analysis [4–7]. Among these applications, terahertz communication is considered crucial for achieving high-speed information transmission in future wireless communication systems.

As terahertz wave applications advance, more complex optical systems are required. To address the challenges of terahertz system complexity and miniaturization, researchers are developing terahertz-wave integrated circuits [8–10]. In integrated circuits, the functional waveguides such as wave splitters and couplers [11], topological waveguides [12,13], delay devices [14], and resonators

[15,16] are important elements. Among these, frequency-conversion techniques that use waveguides play an important role. Waveguide-embedded frequency conversion enables the transformation of signals between different frequency domains, enabling tailored signal processing for various purposes [17].

Recently, successful frequency conversion was achieved by temporally controlling the structural dispersion in GaAs waveguides [18,19]. During the propagation of terahertz pulses within a GaAs waveguide, structural dispersion can be rapidly modified by illuminating the surface with a femtosecond laser. Such an instantaneous change in the structural dispersion corresponds to a temporal boundary, which causes frequency conversion [20–30]. This method of frequency conversion is a potential candidate for significant functional optical components in future terahertz integrated systems. However, the attenuation of the terahertz pulse as it propagates through the entire waveguide varies depending on the timing of the temporal boundary. This characteristic can be problematic for practical applications. For example, in the application of amplitude-modulated

\*Corresponding author. miyamaru@shinshu-u.ac.jp

coding terahertz pulse trains [9,31–33], attenuation can significantly distort the relative amplitudes of the pulses in the pulse train. The dependence of the attenuation of the terahertz pulse on the timing of the temporal boundary is caused by the difference in the attenuation constants before and after the temporal boundary. Therefore, it is important to develop a method that can perform frequency conversion without altering the relative output amplitude, regardless of the temporal boundary timing.

To address this issue, we propose a waveguide with a metallic structure to manage the attenuation of terahertz waves during propagation. In a previous study [18], frequency conversion was achieved by optically exciting the bare top surface of a semiconductor waveguide with a metal coating on the bottom surface using a femtosecond laser. This caused a change from a single-sided to a double-sided metallic waveguide within a very short time. In this waveguide, the attenuation is small before the temporal boundary but increases after the temporal boundary owing to the Joule losses of the optically excited carriers. The difference in attenuation before and after the temporal boundary can cause significant distortion of the terahertz pulse shape.

On the top surface of the proposed waveguide, there is a patterned periodic metallic structure consisting of long metallic wires extending in the propagation direction. The metallic pattern is expected to increase conductivity and reduce propagation attenuation after the temporal boundary. On the other hand, before the temporal boundary, the metallic structure itself causes Joule losses, resulting in higher propagation attenuation than that without the metallic structure. Thus, the magnitude of propagation attenuation before and after the temporal boundary can be balanced by the metallic structure. Consequently, the electromagnetic field at any location in the waveguide experiences the same attenuation. In this study, we fabricated a metal-patterned waveguide and experimentally confirmed that terahertz frequency conversion can be achieved with a uniform output amplitude regardless of the location of the terahertz pulse in the waveguide at the temporal boundary.

## II. EXPERIMENT

In the experiments, we used a waveguide fabricated using semi-insulating GaAs (SI-GaAs) as the material. Figures 1(a) and 1(b) illustrate a schematic of the entire waveguide and an enlarged view of the waveguide, respectively. The waveguide has a thickness of  $d = 0.1$  mm and a width of  $w = 1$  mm. Depending on the specific experiment, we fabricated waveguides of varying lengths  $L$ , ranging from 3 to 10 mm. The bottom surface of the waveguide was covered with a metal film (SI-GaAs/50 nm Pt/30 nm Ti/120 nm Au). The top surface of the waveguide was patterned with a metallic structure composed of

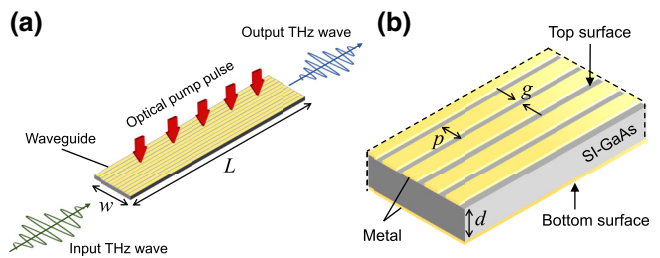


FIG. 1. (a) Schematic of the semiconductor waveguide and optical configuration. The optical pump pulse is irradiated onto the top surface. (b) Enlarged view of the waveguide. The top surface is patterned with a metallic structure. The bottom surface is entirely covered with a metal film.

periodically arranged lines of a metal film (SI-GaAs/10 nm Ti/100 nm Au). The periodicity  $p$  between the metal lines and the gap  $g$  were set to 50 and 4  $\mu\text{m}$ , respectively. The lowest-order diffraction frequency, determined by the period of the metal line, was higher than the terahertz wave frequency of interest in our experiments. We also fabricated the unpatterned waveguide with the same metallic ground for comparison.

We used optical-pump terahertz probe time-domain spectroscopy to generate the temporal boundary and observe the terahertz waveform transmitted through the waveguides. As shown in Fig. 1(a), when a terahertz pulse propagates through the waveguide, the top surface of the waveguide is irradiated with femtosecond optical pump pulses to instantaneously change the structural dispersion. This instantaneous change of the structural dispersion by photoexcitation induces a temporal boundary. The pulse width of the pump pulse was approximately 100 fs. The polarization direction of the pump pulse was perpendicular to the metallic line. The timing of the pump pulses could be arbitrarily controlled by adjusting the delay time  $\tau$  with respect to the terahertz pulse. The incident terahertz pulse was a narrowband pulse with a center frequency of 0.48 THz. The typical relaxation time of photoexcited carriers in GaAs is on the order of nanoseconds in our experiment. This time scale is sufficiently long compared to the time it takes for the terahertz pulse used in the experiment to exit the waveguide after photoexcitation. The polarization of the incident terahertz pulse is parallel to the top and bottom surfaces, which results in the excitation of the transverse electric (TE) mode in the waveguide. Further detailed information regarding other experimental aspects is reported in our previous study [18].

## III. RESULTS AND DISCUSSION

### A. Attenuation constants in the waveguide

Before discussing the experimental results, it is necessary to explain the propagation attenuation in the frequency conversion with a waveguide-type temporal boundary.

During the frequency-conversion process through the temporal boundary, two attenuation constants should be considered: the attenuation constants before ( $\gamma_b$ ) and after ( $\gamma_a$ ) the temporal boundary (see Fig. 2). To investigate these attenuation constants, it was necessary to determine the propagation distance and attenuation of the terahertz pulse intensity before and after the temporal boundary. However, accurately measuring the position of a terahertz pulse within the waveguide when the pump pulse is irradiated is challenging. Therefore, we varied the timing of the pump-pulse irradiation and controlled the relative propagation distance after the temporal boundary.

Figure 2 shows a schematic of the terahertz pulse propagation before and after the temporal boundary. We assume that the center of the terahertz pulse is located at distance  $L_n$  and  $L_0$  from the entrance of the waveguide at the pump timings  $\tau_n$  [Fig. 2(a)] and  $\tau_0$  [Fig. 2(b)], respectively. In this study,  $\tau_0$ , which is the reference for pump timing, can be arbitrarily determined. The intensity  $I_{\text{ON}}^{(n)}$  of the transmitted terahertz pulse for the pump timing  $\tau_n$  can be expressed as follows:

$$I_{\text{ON}}^{(n)} = I_{\text{in}} \eta e^{-\gamma_b L_n} e^{-\gamma_a (L - L_n)}, \quad (1)$$

where  $I_{\text{in}}$  and  $\eta$  represent the incident terahertz pulse intensity and frequency-conversion efficiency, respectively.

By measuring  $I_{\text{ON}}^{(n)}$  for  $\tau_n$  and  $\tau_0$ , the ratio between  $I_{\text{ON}}^{(n)}$  and  $I_{\text{ON}}^{(0)}$  is expressed as follows:

$$\frac{I_{\text{ON}}^{(n)}}{I_{\text{ON}}^{(0)}} = e^{-(\gamma_a - \gamma_b) \{- (L_n - L_0)\}} = e^{-\Delta\gamma(-\Delta L)}, \quad (2)$$

where  $\Delta\gamma = \gamma_a - \gamma_b$  is the difference between the attenuation constants before and after the temporal boundary, and  $\Delta L = L_n - L_0$  is the relative propagation distance. The value of  $\Delta L$  can be derived from the relative pump timing  $\Delta\tau = \tau_n - \tau_0$  and the group velocity before the temporal boundary  $v_g$  as follows:

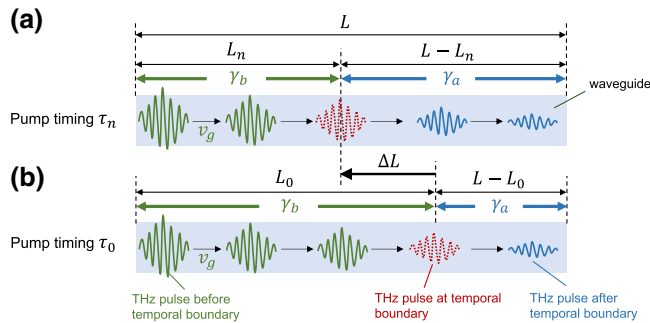


FIG. 2. Schematic of the propagation of a terahertz pulse before and after the temporal boundary ( $\gamma_b$  and  $\gamma_a$  are the attenuation constants before and after the temporal boundary, respectively). Panels (a) and (b) show the pump timing of  $\tau_n$  and  $\tau_0$ , respectively.

$$\Delta L = v_g \Delta\tau, \quad (3)$$

where  $v_g$  is obtained from the dispersion relation of the waveguide mode, as explained in detail in the Supplemental Material [34]. In the actual experiment, we measured  $I_{\text{ON}}^{(n)}$  for several pump timings  $\tau_n$  and obtained  $\Delta\gamma$ .

## B. Converted frequencies

First, we confirmed that the metallic structure did not affect the converted frequency. Figures 3(a) and 3(b) show the transmitted terahertz pulses for the unpatterned and metal-patterned waveguides, respectively, as  $\Delta\tau$  is varied. In this experiment, the pump pulse fluence is  $2.1 \mu\text{J}/\text{mm}^2$ , and the waveguide length is  $L = 5 \text{ mm}$  for both waveguides. The full width at half maximum of the incident terahertz pulse is contained within the waveguide irradiated by the pump pulse at  $\Delta\tau = 0$ . At the bottom of the graphs, the transmitted terahertz pulse without photoexcitation is shown. Figures 3(c) and 3(d) show the corresponding Fourier-transform (FT) power spectra of Figs. 3(a) and 3(b), respectively. It can be observed that the peak frequency in the presence of photoexcitation is converted to a higher frequency (0.55 THz) than that without photoexcitation (0.48 THz) in both waveguides.

The validity of these experimental results was confirmed using a dispersion relation. Figure 3(e) shows the dispersion relations of the lowest-order TE mode in the metal-patterned (blue dash-dotted line), unpatterned (red solid line), and double-metallized (black dashed line) waveguides. These dispersion relations were numerically calculated using COMSOL Multiphysics and determined by the geometrical shape of the waveguide, the metal pattern on the waveguide surface, and the refractive index of the dielectric material. The details of this calculation are provided in the Supplemental Material [34].

The dispersion relations of the double-metallized waveguide corresponded to the states after photoexcitation for both the unpatterned and metal-patterned waveguides, whereas others corresponded to those before photoexcitation for each waveguide. Because of the metallic structure, the dispersion relation of the metal-patterned waveguide underwent a slight change from that of the unpatterned waveguide. The relationship between the input and converted frequencies is determined by these dispersion relations depending on  $k_z$  once the waveguide is fabricated. The experimentally obtained peak frequencies of the output terahertz waves are also plotted for the unpatterned (orange circles) and metal-patterned waveguides (green squares). The filled and open markers of these experimental results are for the output terahertz waves with and without photoexcitation, respectively. The wavenumber was estimated from the theoretical dispersion relation and the experimentally obtained frequency without photoexcitation. The same wavenumber was applied to plot

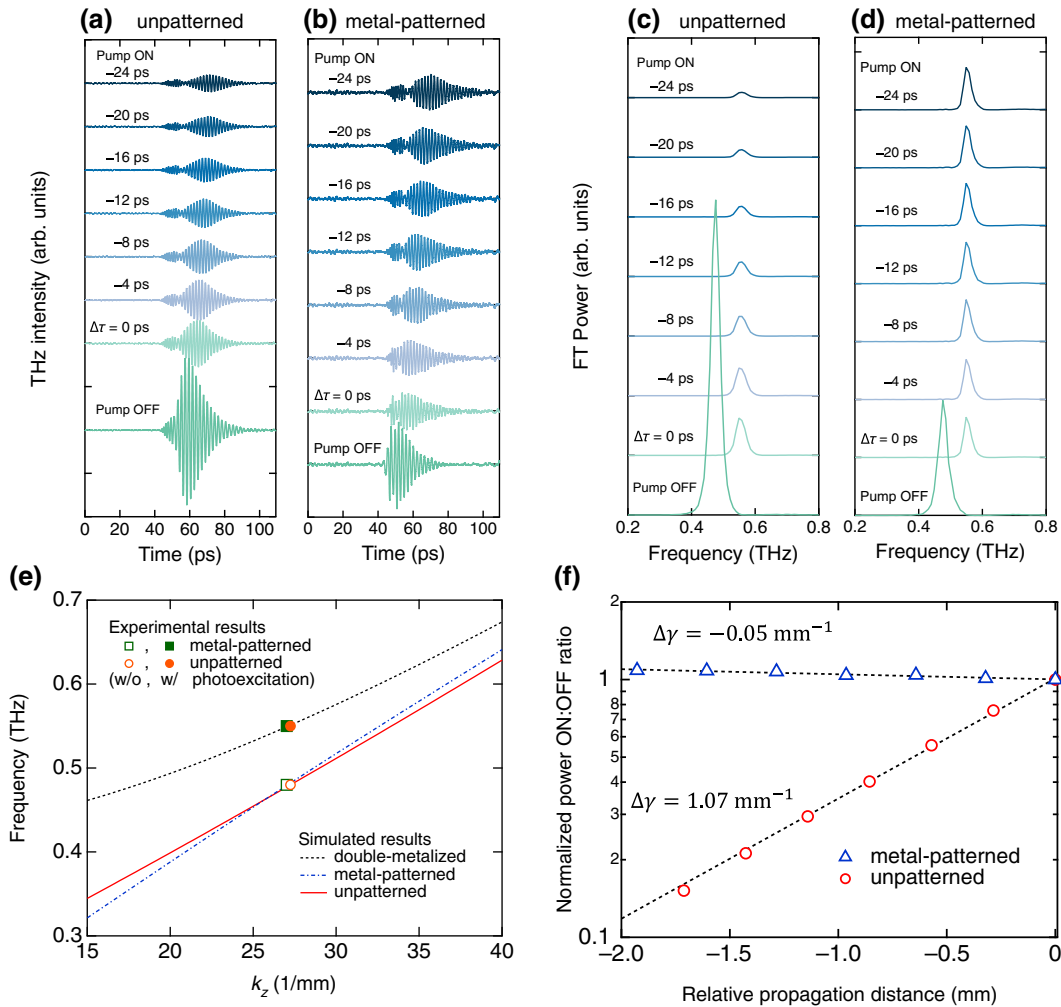


FIG. 3. (a),(c) Pump timing dependence of the transmitted terahertz waveforms and the FT spectra for the unpatterned waveguide. (b),(d) Similar waveforms and FT spectra for the metal-patterned waveguides. (e) Simulated dispersion relations of the lowest-order TE modes in the metal-patterned (blue dash-dotted line), unpatterned (red solid line), and double-metallized (black dashed line) waveguides. The experimentally obtained input and output frequencies are also plotted for the metal-patterned (green squares) and unpatterned (orange circles) waveguides. The filled and open markers for these experimental results are for the output terahertz waves with and without photoexcitation, respectively. (f) Dependence of the ON:OFF ratio on the relative propagation distance for unpatterned (red circles) and metal-patterned (blue triangles) waveguides. The relative propagation distance is determined based on the relative pump timing  $\Delta\tau$  and the group velocity  $v_g$ . Dotted lines represent the fitting of experimental data with exponential functions.

the points with photoexcitation. The experimental results for both waveguides agree well with the theoretical calculations, indicating that the converted frequency is not disturbed by the metallic structure.

Here, we should mention the efficiency of the frequency conversion at the temporal boundary. As previously mentioned, the converted frequency was not affected by the presence of the metal structure. However, the frequency conversion efficiency changed slightly when compared to that of the unpatterned waveguide. The conversion efficiency is determined by the degree of overlap between the spatial distributions of the electromagnetic fields before and after the temporal boundary. From the theoretical analysis, the energy conversion efficiency for the 0.48-THz

incident frequency can be estimated to be  $\eta = 0.76$  and  $0.55$  for the unpatterned and metal-patterned waveguides, respectively. The details for calculating the conversion efficiency are provided in the Supplemental Material [34]. The lower conversion efficiency of the metal-patterned waveguide is attributed to the concentration of electromagnetic fields near the gap, resulting in a reduced overlap with the electromagnetic fields after the temporal boundary.

### C. Dependence of the output terahertz pulse amplitude on pump timing

Subsequently, we focused on the change in the output terahertz wave amplitude depending on the pump timing.

The purpose of this study is to balance  $\gamma_a$  and  $\gamma_b$  to achieve  $\Delta\gamma = 0$ . In the time-domain waveform data, the amplitude of the output terahertz pulse decreased for the unpatterned waveguide as the timing of the pump pulse becomes earlier [Fig. 3(a)]. On the other hand, the change in amplitude after frequency conversion is gradual for the metal-patterned waveguide [Fig. 3(b)]. These results imply the following: In the unpatterned waveguide, the output terahertz pulse amplitude varied significantly depending on the position of the terahertz pulse at pump timing. In contrast, in the metal-patterned waveguide, the output terahertz pulse amplitude remained almost constant regardless of the position of the terahertz pulse at the pump timing. This indicates that the pulse shape was preserved even when a terahertz pulse with a wider pulse width was used, or relative amplitudes of a terahertz pulse train were preserved.

From the results shown in Figs. 3(c) and 3(d), we plot the ON:OFF ratio as a function of the relative propagation distance after photoexcitation, as shown in Fig. 3(f). The ON:OFF ratio is defined as the ratio of the spectrally integrated fitted curve when the optical pump is ON to that when the pump is OFF. The fitting function was the square of the Lorentz function because we used double bandpass filters to restrict the bandwidth of the incident terahertz pulse. The relative propagation distance  $\Delta L$  was calculated from  $\Delta\tau$  and the group velocity of  $0.238c_0$  and  $0.268c_0$  for the unpatterned and metal-patterned waveguides [34], respectively, where  $c_0$  is the speed of light in vacuum.

The ON:OFF ratio is normalized by that at  $\Delta L = 0$  for each waveguide to obtain the values corresponding to Eq. (2). The vertical axis in Fig. 3(f) represents a logarithmic scale. The ON:OFF ratio decays with increasing the absolute value of the propagation distance for the unpatterned waveguide (red circles). In contrast, the ON:OFF ratio of the metal-patterned waveguide increases slightly (blue triangles). From these results, the value of  $\Delta\gamma$  can be estimated by fitting the experimental data with an exponential function (dotted lines). The obtained  $\Delta\gamma$  are  $1.07$  and  $-0.05 \text{ mm}^{-1}$  for the unpatterned and metal-patterned waveguides, respectively. For the metal-patterned waveguide,  $\gamma_a$  and  $\gamma_b$  are nearly balanced owing to the metallic structure, and correspondingly  $\Delta\gamma$  becomes nearly zero.

The value of  $\Delta\gamma$  becomes zero owing to the metallic structure, as explained below. First, let us consider  $\gamma_b$ . The value of  $\gamma_b$ , which corresponds to the propagation loss before the temporal boundary, is determined by the structure of the waveguide. The value of  $\gamma_b$  can be experimentally obtained by measuring the intensity of the terahertz pulses that passed through waveguides of different lengths. The FT intensity of the transmitted terahertz pulse as a function of the waveguide length for the unpatterned (red circles) and metal-patterned (blue triangles) waveguides is plotted in Fig. 4. The vertical axis in the figure represents a logarithmic scale. For both waveguides,

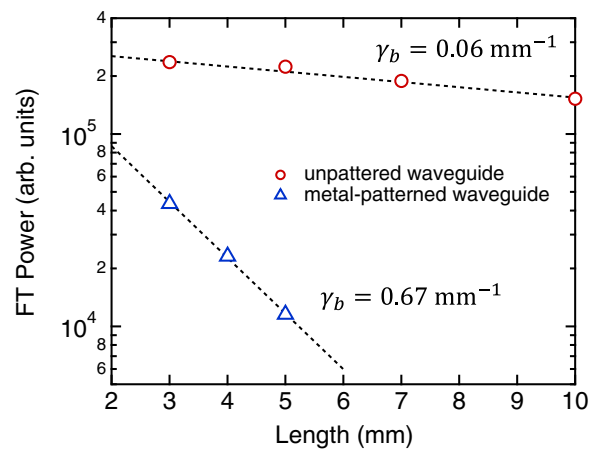


FIG. 4. Integrated FT power of the transmitted terahertz wave as a function of the waveguide length for the unpatterned (red circles) and metal-patterned (blue triangles) waveguides.

decayed exponentially as the waveguide length increased. By fitting these results with an exponential function (dotted lines), we can estimate the value of  $\gamma_b$  to be  $0.67$  and  $0.06 \text{ mm}^{-1}$  for the metal-patterned and unpatterned waveguides, respectively. Compared to the unpatterned waveguide,  $\gamma_b$  of the metal-patterned waveguide is relatively higher. According to the results obtained from finite-element simulations, this attenuation was attributed to Joule loss in the deposited metal. A detailed description of the simulation method is provided in the Supplemental Material [34].

The value of  $\gamma_a$  can be obtained from  $\gamma_a = \Delta\gamma + \gamma_b$ , and it is calculated to be  $1.13$  and  $0.62 \text{ mm}^{-1}$  for the unpatterned and metal-patterned waveguides, respectively. These results are summarized in Table I. In contrast to  $\gamma_b$ , the value of  $\gamma_a$  is lower for the metal-patterned waveguide. This is because the Joule loss caused by the optically excited carriers after photoexcitation is reduced by patterning the metal structure.

According to the experimental results, the following conclusions were drawn. The values of  $\gamma_b$  and  $\gamma_a$  were significantly different for the unpatterned waveguide ( $\gamma_b < \gamma_a$ ). By patterning the metallic structure,  $\gamma_b$  increases and  $\gamma_a$  decreases from those of the unpatterned waveguide, resulting in a balance between the two values. In practical applications, the balanced values of  $\gamma_b$  and  $\gamma_a$  should be as

TABLE I. Measured attenuation constants for unpatterned and metal-patterned waveguides.

Waveguide	Attenuation constant ( $\text{mm}^{-1}$ )		
	$\gamma_b$	$\gamma_a$	$\Delta\gamma$
Unpatterned	0.06	1.13	1.07
Metal-patterned	0.67	0.62	-0.05

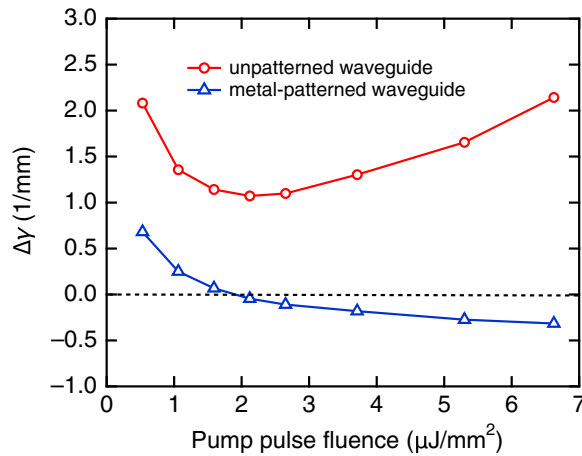


FIG. 5. Pump pulse fluence dependence of  $\Delta\gamma$  for the unpatterned (red circles) and metal-patterned (blue triangles) waveguides.

small as possible. Regarding  $\gamma_b$ , the value of the attenuation constant can be decreased by decreasing the resistance of the patterned metal. This can be achieved by increasing the thickness of the patterned metal [34] or using a metal with higher conductivity.

#### D. Dependence on pump pulse fluence and tunability of $\Delta\gamma$

Finally, we discuss the tunability of  $\Delta\gamma$  by investigating the dependence on pump pulse fluence. The value of  $\gamma_a$  varies with the pump pulse fluence, while the value of  $\gamma_b$  remains fixed once the metallic structure is fabricated. This is because  $\gamma_a$  is dominantly attributed to the Joule loss of photoexcited carriers. At low pump pulse fluences, the photoexcited carrier concentration is low, resulting in low conductivity, and hence a high attenuation constant. As the pump pulse fluence increased, it was expected that the conductivity would increase and the attenuation constant would decrease. The values of  $\Delta\gamma$  are plotted in Fig. 5 as a function of pump pulse fluence for the unpatterned (red circles) and metal-patterned waveguides (blue triangles). For the unpatterned waveguide,  $\Delta\gamma$  always has a positive value at any pump pulse fluence. For the metal-patterned waveguide, as the pump pulse fluence increases,  $\Delta\gamma$  decreases and reaches zero at approximately 2  $\mu\text{J/mm}^2$ , indicating that  $\gamma_a$  becomes equal to  $\gamma_b$ . Figure 3 shows the experimental results obtained for this pump fluence range. The result of this pump pulse fluence dependence indicates the tunability of  $\Delta\gamma$  by adjusting the pump fluence.

Here, as the pump fluence increases more than 2  $\mu\text{J/mm}^2$ ,  $\gamma_a$  increases for the unpatterned waveguides, while  $\Delta\gamma$  decreases for the metal-patterned waveguide. The reason for the increase in the attenuation constant of

the unpatterned waveguide is not clear at this stage. However, at exceptionally high pump pulse fluences beyond the linear absorption regime, the strong nonlinearity in the optical absorption of GaAs may contribute to the experimentally observed increase in loss [35]. Further theoretical developments are required to elucidate the reasons for these characteristics.

#### IV. CONCLUSION

This study presents a method for balancing propagation losses before and after the temporal boundary in frequency conversion through the patterning of a metallic structure on the top surface of a waveguide. The presence of a metallic structure reduces the area of the semiconductor surface irradiated by the pump pulse, increasing the average conductivity and reducing the Joule losses after the temporal boundary. In contrast, the propagation loss before the temporal boundary increases owing to the Joule loss of the patterned metal itself. These characteristics balance the attenuation constants before and after the temporal boundary at an appropriate pump fluence. In this case, the amplitude of the output terahertz pulse remained constant, regardless of the location of the terahertz pulse within the waveguide at the pump timing.

The frequency-conversion method utilizing the waveguide and temporal boundary can be applied to a wide range of terahertz frequencies (0.1–10 THz), as long as the real part of the dielectric constant of the photoexcited GaAs has a negative value. Therefore, the results of this study are significant for future terahertz integrated circuits, as they can be used as functional components with frequency-conversion capabilities. For example, when using terahertz pulses with a wide pulse width, they can be converted from one frequency pulse to another while maintaining the pulse shape. In another example, in information processing involving multiple pulses or pulse trains, it is believed that the input pulse trains can be converted into other frequency pulse trains while maintaining the relative amplitude ratio of the input pulse trains. Thus, a deeper understanding of waveguides with metal structures can provide important insights for exploring new applications and designing devices.

#### ACKNOWLEDGMENTS

This work was partially supported by JSPS KAKENHI Grants No. 22K04964 and No. 22K20493. F.M. was supported by Inamori foundation. K.T. was partially supported by a research grant from Takano Gakujutsu-Shinko-Zaidan. Y.N. was supported by JST PRESTO Grant No. JPMJPR20L6. J.P.-U., J.M., and K.M.D. are supported by the Femtosecond Spectroscopy Unit at Okinawa Institute of Science and Technology Graduate University. F.M. also acknowledges Professor Masahiko Higuchi at Shinshu University for fruitful discussions.

- [1] T. Nagatsuma, G. Ducournau, and C. C. Renaud, Advances in terahertz communications accelerated by photonics, *Nat. Photonics* **10**, 371 (2016).
- [2] K. Yamamoto, M. Yamaguchi, F. Miyamaru, M. Tani, M. Hangyo, T. Ikeda, A. Matsushita, K. Koide, M. Tatsuno, and Y. Minami, Noninvasive inspection of C-4 explosive in mails by terahertz time-domain spectroscopy, *Jpn. J. Appl. Phys.* **43**, L414 (2004).
- [3] J. F Federici, B. Schulkin, F. Huang, D. Gary, R. Barat, F. Oliveira, and D. Zimdars, THz imaging and sensing for security applications—Explosives, weapons and drugs, *Semicond. Sci. Technol.* **20**, S266 (2005).
- [4] K. Kawase, Y. Ogawa, Y. Watanabe, and H. Inoue, Non-destructive terahertz imaging of illicit drugs using spectral fingerprints, *Opt. Express* **11**, 2549 (2003).
- [5] T. Kiwa, T. Kamiya, T. Morimoto, K. Sakai, and K. Tsukada, pH measurements in 16-nL-volume solutions using terahertz chemical microscopy, *Opt. Express* **26**, 8232 (2018).
- [6] P. Klarskov, H. Kim, V. L. Colvin, and D. M. Mittleman, Nanoscale laser terahertz emission microscopy, *ACS Photonics* **4**, 2676 (2017).
- [7] T. Kiwa, Y. Kondo, Y. Minami, I. Kawayama, M. Tonouchi, and K. Tsukada, Terahertz chemical microscope for label-free detection of protein complex, *Appl. Phys. Lett.* **96**, 211114 (2010).
- [8] K. Sengupta, T. Nagatsuma, and D. M. Mittleman, Terahertz integrated electronic and hybrid electronic-photonic systems, *Nat. Electron.* **1**, 622 (2018).
- [9] A. Herter, A. Shams-Ansari, F. F. Settembrini, H. K. Warner, J. Faist, M. Lončar, and I.-C. Benea-Chelmus, Terahertz waveform synthesis in integrated thin-film lithium niobate platform, *Nat. Commun.* **14**, 11 (2023).
- [10] R. A. S. D. Koala, M. Fujita, and T. Nagatsuma, Nanophotonics-inspired all-silicon waveguide platforms for terahertz integrated systems, *Nanophotonics* **11**, 1741 (2022).
- [11] K. S. Reichel, R. Mendis, and D. M. Mittleman, A broadband terahertz waveguide T-junction variable power splitter, *Sci. Rep.* **6**, 28925 (2016).
- [12] J. Webber, Y. Yamagami, G. Ducournau, P. Sriftgiser, K. Iyoda, M. Fujita, T. Nagatsuma, and R. Singh, Terahertz band communications with topological valley photonic crystal waveguide, *J. Lightwave Tech.* **39**, 7609 (2021).
- [13] A. Kumar, M. Gupta, P. Pitchappa, N. Wang, M. Fujita, and R. Singh, Terahertz topological photonic integrated circuits for 6G and beyond: A perspective, *J. Appl. Phys.* **132**, 140901 (2022).
- [14] F. Miyamaru, H. Morita, Y. Nishiyama, T. Nishida, T. Nakanishi, M. Kitano, and M. W. Takeda, Ultrafast optical control of group delay of narrow-band terahertz waves, *Sci. Rep.* **4**, 4346 (2014).
- [15] P. A. George, C. Manolatou, F. Rana, A. L. Bingham, and D. R. Grischkowsky, Integrated waveguide-coupled terahertz microcavity resonators, *Appl. Phys. Lett.* **91**, 191122 (2007).
- [16] J. Xie, X. Zhu, X. Zang, Q. Cheng, L. Chen, and Y. Zhu, Terahertz integrated device: High-*Q* silicon dielectric resonators, *Opt. Mat. Express* **8**, 50 (2018).
- [17] H. Zeng, H. Liang, Y. Zhang, L. Wang, S. Liang, S. Gong, Z. Li, Z. Yang, X. Zhang, F. Lan, Z. Feng, Y. Gong, Z. Yang, and D. M. Mittleman, High-precision digital terahertz phase manipulation within a multichannel field perturbation coding chip, *Nat. Photonics* **15**, 751 (2021).
- [18] F. Miyamaru, C. Mizuo, T. Nakanishi, Y. Nakata, K. Hasebe, S. Nagase, Y. Matsubara, Y. Goto, J. Pérez-Urquiza, J. Madéo, and K. M. Dani, Ultrafast Frequency-Shift Dynamics at Temporal Boundary Induced by Structural-Dispersion Switching of Waveguides, *Phys. Rev. Lett.* **127**, 053902 (2021).
- [19] K. Takano, S. Uchiyama, S. Nagase, Y. Tsuchimoto, T. Nakanishi, Y. Nakata, J. Pérez-Urquiza, J. Madéo, K. M. Dani, and F. Miyamaru, Frequency down-conversion of terahertz waves at optically induced temporal boundary in GaAs waveguides (unpublished).
- [20] S. C. Wilks, J. M. Dawson, and W. B. Mori, Frequency Up-Conversion of Electromagnetic Radiation with Use of an Overdense Plasma, *Phys. Rev. Lett.* **61**, 337 (1988).
- [21] Y. Xiao, G. P. Agrawal, and D. N. Maywar, Spectral and temporal change of optical pulses propagating through time-varying linear media, *Opt. Lett.* **36**, 505 (2011).
- [22] S. P. Kuo, Frequency Up-Conversion of Microwave Pulse in a Rapidly Growing Plasma, *Phys. Rev. Lett.* **65**, 1000 (1990).
- [23] S. P. Kuo, A. Ren, and G. Schmidt, Frequency downshift in rapidly ionizing media, *Phys. Rev. E* **49**, 3310 (1994).
- [24] N. Yugami, T. Niizuma, T. Higashiguchi, H. Gao, S. Sasaki, H. Ito, and Y. Nishida, Experimental observation of short-pulse upshifted frequency microwaves from a laser-created overdense plasma, *Phys. Rev. E* **65**, 036505 (2002).
- [25] J. Faith, S. P. Kuo, and J. Huang, Frequency downshifting and trapping of an electromagnetic wave by a rapidly created spatially periodic plasma, *Phys. Rev. E* **55**, 1843 (1997).
- [26] S. P. Kuo and J. Faith, Interaction of an electromagnetic wave with a rapidly created spatially periodic plasma, *Phys. Rev. E* **56**, 2143 (1997).
- [27] A. Nishida, N. Yugami, T. Higashiguchi, T. Otsuka, F. Suzuki, M. Nakata, Y. Sentoku, and R. Kodama, Experimental observation of frequency up-conversion by flash ionization, *Appl. Phys. Lett.* **101**, 161118 (2012).
- [28] J. Upham, Y. Tanaka, T. Asano, and S. Noda, On-the-fly wavelength conversion of photons by dynamic control of photonic waveguides, *Appl. Phys. Express* **3**, 062001 (2010).
- [29] T. Kampfrath, D. M. Beggs, T. P. White, A. Melloni, T. F. Krauss, and L. Kuipers, Ultrafast adiabatic manipulation of slow light in a photonic crystal, *Phys. Rev. A* **81**, 043837 (2010).
- [30] K. Lee, H. Son, J. Park, B. Kang, W. Jeon, F. Rotermund, and B. Min, Linear frequency conversion via sudden merging of meta-atoms in time-variant metasurfaces, *Nat. Photonics* **12**, 765 (2018).
- [31] J. E. Nkeck, L.-P. Bélineau, X. Ropagnol, D. Deslandes, D. Morris, and F. Blanchard, Parallel generation and coding of a terahertz pulse train, *APL Photonics* **7**, 126105 (2022).
- [32] Q. Tian, H. Xu, Y. Wang, Y. Liang, Y. Tan, X. Ning, L. Yan, Y. Du, R. Li, J. Hua, W. Huang, and C. Tang,

- Efficient generation of a high-field terahertz pulse train in bulk lithium niobate crystals by optical rectification, *Opt. Express* **29**, 9624 (2021).
- [33] L. Gingras and D. G. Cooke, Direct temporal shaping of terahertz light pulses, *Optica* **4**, 1416 (2017).
- [34] See Supplemental Material at <http://link.aps.org-supplemental/10.1103/PhysRevApplied.21.044044> for detailed discussion on the calculation of dispersion relation and estimation of group velocity, calculation of conversion efficiency, and dependence of the attenuation constant on metal conductivity.
- [35] F. Kadlec, H. Němec, and P. Kužel, Optical two-photon absorption in GaAs measured by optical-pump terahertz-probe spectroscopy, *Phys. Rev. B* **70**, 125205 (2004).